A New Method of Direct Time-Domain Simulations of an UWB Transmission for an Electromagnetic Wave Source Placed on a Convex Obstacle

P. Górniak[1] W. Bandurski[1]

Abstract – **The paper presents a new approach to time-domain effective simulation of ultra-wideband (UWB) electromagnetic (EM) wave propagation when a source is placed on convex obstacle. The frequency domain uniform theory of diffraction (UTD) and rational approximation exploiting the vector fitting algorithm (VF) is used for deriving the closed form time domain functions of the radiated and coupled fields.**

1 INTRODUCTION

Ultra-wideband (UWB) technology can be used in many applications in telecommunication area [1]. However due to its large bandwidth feature careful analysis of a given UWB system is required, in particular analysis of the propagation channel.

In this paper we focus our analysis on effective time domain modeling of propagation of UWB electromagnetic wave when a source is placed on a convex conducting elliptical cylinder. We consider coupling as well as radiation scenarios. W simplify our analysis to a 2 dimensional scenario but our results can be adopted also to a 3D scenario. We use the Uniform Theory of Diffraction (UTD) in our analysis. The convex objects in the form of elliptical cylinders, in practice, can be used effectively to model the convex obstacle such as a human body what was shown in e.g. [2, 3] for the scenario of wireless body area networks (WBAN) including the model given in Fig. 1. We present closed form impulse responses of UTD rays dedicated for the radiation and the coupling scenarios. For the sake of clarity and simplicity of the description of our approach we consider the TE polarization case only (taking into account z-directed magnetic current source placed at point Q', Fig. 1).

The problem of the analytical description of propagation of EM fields generated by sources placed on a convex surface in the time and the frequency domain was considered in the literature, e.g. [2, 4, 5]. Although the solutions presented in these papers provide great accuracy of simulations, long time of computations can be associated with them.

As a similarly accurate and much less complex solution, we introduce a universal rational approximations (for direct and creeping rays) which are independent of geometry of the propagation scenario, and of the frequency band. For this purpose, we introduce new variables for which we carry out universal rational approximations by means of the VF algorithm [6]. These new variables depend on the frequency and the geometry of the propagation scenario. Using this approach we have to perform the rational approximations once for a radiation ray (e.g. the ray heading form Q' to PL or from Q' to QR' in Fig. 1) and coupling ray (e.g. the ray heading form QR' to PR in Fig. 1). The obtained coefficients can be then used in many other scenarios and frequency ranges. In this way we obtain universal approximations which can be used for all considered (predefined) parameters of scenario geometries and frequency bands.

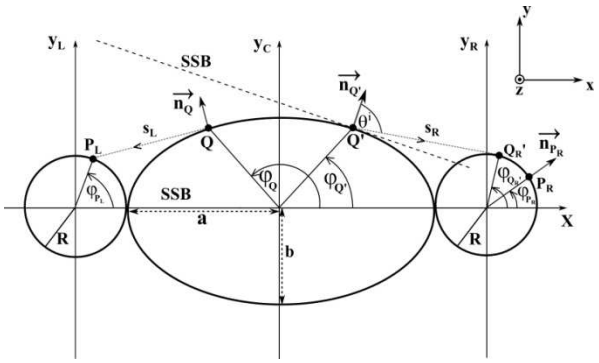

Figure 1: The example 2D ray scenario of a propagation of electromagnetic wave on a convex body. The EM wave is radiated by z-directed magnetic current source placed at point Q'. The observation points are placed at point P_L and point P_R.

2 THE TRANSFER FUNCTIONS OF RAYS

The exemplary scenario of radiation and coupling rays is shown in Fig. 1. The position of a z-directed magnetic current source is at the point Q'. We can distinguish three kinds of UTD rays. The first of them is a radiation direct ray which travels between the points Q' to Q_R'. The second kind is a radiation creeping ray which travels between the points Q' to P_L. The last kind of a ray is a coupling ray which originates at the point Q_R' and leads to the point P_R. The counterclockwise shedding point is marked with Q. The main parameters of the scenario are: a, b – the axes of the elliptical cylinder, R – the radius circular cylinder, $\varphi_{Q'}$, φ_Q, $\varphi_{Q_R'}$, φ_{P_R} – the coordinates of attachment and shedding points that define a creeping wave path, θ^i – the angle between vector $\overrightarrow{n_{Q'}}$ and the direct ray originating at Q' (Fig. 1). The distances along which the EM wave propagates in the air are denoted by s_L and s_R. The electric field vectors

[1] Faculty of Electronics and Telecommunications, Poznan University of Technology, Pl. M. Sklodowskiej-Curie 5, 60-965 Poznan, Poland, e-mail: pgorniak@et.put.poznan.pl, tel.: +48 616653898.

The presented work has been funded by the Polish Ministry of Science and Higher Education within the status activity task 2015 in "Development of methods for the analysis of propagation and signal processing as well as EMC issues"

associated with a radiation and a coupling ray at the observation points P_L and P_R are parallel to the unit vectors $\overrightarrow{n_Q}$ and $\overrightarrow{n_{P_R}}$, respectively.

Fourier transforms of the time-domain derivative of a TE polarized magnetic current source – M(ω) and the electric filed at the observation point P_L – $E^{P_L}(\omega)$ and at the observation point P_R – $E^{P_R}(\omega)$ are related by (1) and (2), respectively [7]:

$$E^{P_L}(\omega) = M(\omega)H^c_{rad}(\omega)A_c(s_L)exp\left(\frac{-j\omega s_{pL}}{v_0}\right), \quad (1)$$

$$E^{P_R}(\omega) = M(\omega)H^i_{rad}(\omega)H_{cpl}(\omega)A_c(s_R)exp\left(\frac{-j\omega s_{pR}}{v_0}\right). \quad (2)$$

where s_{pL} and s_{pR} are the total lengths of the rays originating at point Q' and terminating at the points P_L and P_R, respectively, v_o is the speed of EM wave in free space, $A_c(s_L)$ and $A_c(s_R)$ are equal to $(s_L)^{-0.5}$ and $(s_R)^{-0.5}$, respectively [7]. Transfer functions $H^c_{rad}(\omega)$ and $H^i_{rad}(\omega)$ are associated with a creeping radiation ray and a direct radiation ray, respectively while $H_{cpl}(\omega)$ relates to a coupling ray that originates at the point $Q_{R'}$. The three outlined transfer functions will be approximated in the next section of the paper with the VF algorithm. The transfer functions $H^c_{rad}(\omega)$ and $H^i_{rad}(\omega)$ are defined with the universal Fock radiation function while $H_{cpl}(\omega)$ with the Fock coupling function [7]. These free functions will be now rearranged to enable their approximation with rational functions using the VF algorithm [6]. We will express them as functions of new variables (normalized frequencies). For the case of TE polarized magnetic current source transfer functions $H^c_{rad}(\omega)$, $H^i_{rad}(\omega)$ and $H_{cpl}(\omega)$ can be rearranged into the following form:

$$H^c_{rad}(\xi^c_{sub}) = -\sqrt{\frac{1}{4\pi \cdot R_e{\theta_c}^3}} \times exp(j\pi/4)\sqrt{\xi^c_{sub}} \cdot G\left({\xi^c_{sub}}^{1/3}\right), \quad (3)$$

$$H^i_{rad}(\xi^i_{sub}) = -\sqrt{\frac{1}{4\pi \cdot cos^3(\theta^i)a_e(Q')}} \times exp(j\pi/4)\sqrt{-\xi^i_{sub}} \cdot G\left({\xi^i_{sub}}^{1/3}\right), \quad (4)$$

$$H_{cpl}(\xi^c_{sub}) = -\frac{1}{\sqrt{\pi} \cdot {\theta_c}^2 {R_e}^{2/3}[a_e(Q')a_e(Q)]^{1/6}} \times exp(j\pi/4)\sqrt{\xi^c_{sub}} \cdot V\left({\xi^c_{sub}}^{1/3}\right), \quad (5)$$

where:

$$\xi^c_{sub} = \frac{\omega R_e}{2v_0}{\theta_c}^3, \quad (6)$$

$$\xi^i_{sub} = -\frac{\omega a_e(Q')}{2v_0}cos^3(\theta^i), \quad (7)$$

$$\theta_c = a \cdot b \cdot F_c\sqrt{T_c}, \quad (8)$$

$$R_e = \left(\frac{1}{\sqrt{T_c}}\right)^3 \cdot \frac{1}{a \cdot b}. \quad (9)$$

Definitions of variables T_c and F_c can be found in APPENDIX I of the paper while $a_e(Q')$ and $a_e(Q)$ are the radii of curvature of the elliptical cylinder cross-section at the attachment point (Q') and the shedding point (Q), respectively (the termination points for a creeping path) [7]. It should be noted that for the case of a creeping wave propagating along the right circular cylinder in Fig. 1 points Q' and Q become points $Q_{R'}$ and P_R, respectively. The rest of the variables used in the above equations are illustrated in Fig. 1. Functions G(x) and V(x) are the universal Fock radiation and coupling function for the TE polarization case, respectively. It should be noted that when $a = b = R$ (circular cylinder case), R_e simplifies to R while θ_c is equal the angle distance that travels a creeping ray along a convex obstacle surface.

In order to find the universal VF approximation of (3) – (5) dedicated to general, practical UWB scenarios we rewrite (3) – (5) by defining new functions of the new presented above variables which will by approximated then with the VF algorithm.

$$H^c_{rad}(\xi^c_{sub}) = \sqrt{\frac{1}{4\pi \cdot R_e{\theta_c}^3}} \cdot U^c_{rad}(\xi^c_{sub}), \quad (10)$$

$$H^i_{rad}(\xi^i_{sub}) = \sqrt{\frac{1}{4\pi \cdot cos^3(\theta^i)a(Q')}} \cdot U^i_{rad}(\xi^i_{sub}), \quad (11)$$

$$H_{cpl}(\xi^c_{sub}) = \frac{1}{\sqrt{\pi} \cdot {\theta_c}^2 {R_e}^{2/3}[a(Q')a(Q)]^{1/6}} \cdot U_{cpl}(\xi^c_{sub}). \quad (12)$$

It should be noted that the expressions which are multiplied by the new functions of the new variables are independent of frequency.

The analogous formulas to the three above equations for the case of TM polarized magnetic current source as well as the case of an electric current source are not given in the paper but can be found easily using the theory presented in e.g. [7].

3 RATIONAL APPROXIMATION

In order to find the universal simple in form time domain equivalents of (3) – (5) functions $\boldsymbol{U^c_{rad}(\xi^c_{sub})}$, $\boldsymbol{U^i_{rad}(\xi^i_{sub})}$, and $\boldsymbol{U_{cpl}(\xi^c_{sub})}$ will be approximated with VF algorithm in the predefined domain limits.

We determine the ranges of the variables $\boldsymbol{\xi^c_{sub}}$ and $\boldsymbol{\xi^i_{sub}}$. These ranges should reflect the practical values of parameters of an UWB propagation scenario.

We assume $0.1 \le R_e \le 0.3$ [m] - compare [2, 3], $0.5 \le f \le 10$ [GHz] (typical UWB spectrum), $10^{-4} \le \theta_c \le \pi$ [rad] (from the practically grazing incidence case to the backscattering case) and $0.5 \cdot 10^{-3} \le \boldsymbol{cos(\theta^i)} \le 1$.

With the above assumed bounds for UWB channel scenario parameters the limits of approximation variables are as follows: $10^{-11} \le -\xi^i_{sub} \le 10^2$, $10^{-11} \le \xi^c_{sub} \le 10^3$ (log scale sampling of approximation domains is used).

After performing VF approximations of $U^c_{rad}(\xi^c_{sub})$, $U^i_{rad}(\xi^i_{sub})$, and $U_{cpl}(\xi^c_{sub})$ with the maximum 1% allowed error of approximation in the predefined domains limits we obtained 25, 42 and 25 components approximating $U^c_{rad}(\xi^c_{sub})$, $U^i_{rad}(\xi^i_{sub})$, and $U_{cpl}(\xi^c_{sub})$, respectively. When we use (13) and (14) as variables independent on ω, we can present the approximated forms of (3) – (5) in (15) – (17):

$$\xi^{cw} = \frac{\xi^c_{sub}}{\omega}, \tag{13}$$

$$\xi^{iw} = \frac{\xi^i_{sub}}{\omega}, \tag{14}$$

$$H^c_{rad}(\omega) \approx \sqrt{\frac{1}{4\pi \cdot R_e \theta_c{}^3}} \cdot \sum_{k=1}^{25} \frac{C_{rc(k)}(\xi^{cw})^{-1}}{j\omega + A_{rc(k)}(\xi^{cw})^{-1}}, \tag{15}$$

$$H^i_{rad}(\omega) \approx \sqrt{\frac{1}{4\pi \cdot cos^3(\theta^i) a(Q')}} \cdot \sum_{k=1}^{42} \frac{C_{ri(k)}(\xi^{iw})^{-1}}{j\omega + A_{ri(k)}(\xi^{iw})^{-1}}, \tag{16}$$

$$H_{cpl}(\omega) \approx \frac{1}{\sqrt{\pi} \cdot \theta_c{}^2 R_e^{\frac{2}{3}} [a(Q')a(Q)]^{\frac{1}{6}}} \times \sum_{k=1}^{25} \frac{C_{cpl(k)}(\xi^{cw})^{-1}}{j\omega + A_{cpl(k)}(\xi^{cw})^{-1}}. \tag{17}$$

The corresponding time-domain equivalents of (15) – (17) are the sums of exponential functions, which can be easily found by applying the inverse Laplace transform.

The approximations (15) – (17) and the corresponding time-domain functions are valid when the following inequalities are fulfilled:

$$\frac{10^{-11}}{2\pi f_L} \le \xi^{cw} \le \frac{10^3}{2\pi f_H}, \tag{18}$$

$$\frac{10^{-11}}{2\pi f_L} \le -\xi^{iw} \le \frac{10^2}{2\pi f_H}. \tag{19}$$

where f_L and f_H are the lower and the upper limits of the considered frequency band of a time-domain derivative of a current source.

We set values of f_L and f_H, as these frequencies for which the amplitude of an input signal in the frequency domain decreases to 2% of its maximum value.

3 SPICE MODEL

In this paper propose to use SPICE models associated with the results from Section III. Modeling in SPICE enables the possibility of including detailed models of a transmitter and a receiver that consider their nonlinearities.

As a result of the approximations, described in the previous section, we obtain three transfer functions: $H^c_{rad}(\omega)$, $H^i_{rad}(\omega)$ and $H_{cpl}(\omega)$ (jω = s), as a finite series of partial fractions. They have the form of a single fraction which represents a partial transfer function of the two-port, which are next used to build the subcircuits corresponding to each partial transfer function. The two-ports can be found by adopting the procedure given by us in [8].

4 NUMERICAL EXAMPLES

In this section we verify the results presented in Sections 2 and 3 with implementation of Spice models through simulations of propagation of UWB EM wave on a convex body shown in Fig. 1. The source of a wave is a TE polarized magnetic current source placed on an elliptical cylinder. SPICE simulation results are compared with IFFT results calculated with (1) and (2). We present two numerical examples of the scenario from Fig. 1. As a derivative of a magnetic current source we use an UWB pulse given by (22) with t_c=1ns and τ=0.2ns:

$$m(t) = \left[1 - 4\pi\left(\frac{t - t_c}{\tau}\right)^2\right] \times exp\left[-2\pi\left(\frac{t - t_c}{\tau}\right)^2\right]. \tag{22}$$

In both examples the elliptical cylinder axes are a = 0.3m, b = 0.2m while R is equal 0.1m. In the first example $\varphi_{Q'}$, φ_{P_L} and φ_{P_R} equal $\frac{5}{4}\pi$, $\frac{1}{2}\pi$ and $\frac{1}{4}\pi$ rad, respectively while in the second example these variables equal $\frac{2}{5}\pi$, π and 0 rad, respectively.

The simulation results of the first example are shown in Fig. 2, while the calculation results for the second example are shown in Fig. 3. The propagation delay is not taken into account in presentation of the results. In each figure are shown 2 waveforms (left and right). The left waveform relates to the observation point P_L, while the right waveform is associated with the observation point P_R. Frequencies f_L and f_H are 0.32 GHz and 10.40 GHz, respectively. The solid line waveforms are calculated using IFFT, while the dotted

line waveforms are calculated in SPICE. In both examples IFFT and SPICE simulation results are in very good agreement what is a consequence of the fact that ranges of ξ^{cw} and $-\xi^{iw}$ for the given ray scenarios fit in the limits given in Section 3.

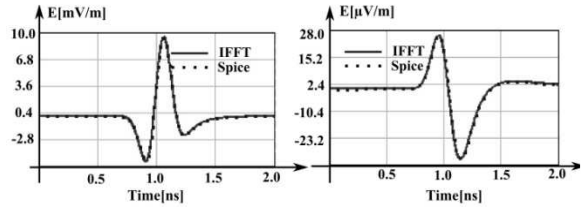

Figure 2: The simulation results at the observation point P_L in Fig. 1 (left waveform) and at the observation point P_R in Fig. 1 (right waveform) for the first example.

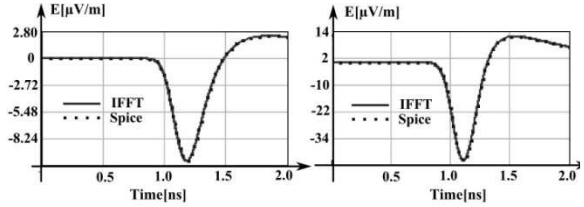

Figure 3: The simulation results at the observation point P_L in Fig. 1 (left waveform) and at the observation point P_R in Fig. 1 (right waveform) for the second example

Comparing the time efficiency of calculations we can report that frequency-domain and IFFT based calculations require 5-10 times more time than Spice simulations. These numbers grows up to several tens (e.g. 80) when algorithms implementing only analytical calculations are applied.

5 CONCLUSIONS

In the paper we presented universal rational approximations of transfer functions of UTD rays associated with a propagation of an UWB electromagnetic wave when a source is placed on a convex obstacle. In order to obtain universal vector fitting approximations we introduced new variables. We specified the ranges of these new variables that reflect practical values of UWB propagation scenarios. Various scenarios of UWB EM wave propagation in a proximity of and on a convex body for various frequency bands can be modeled with our results by controlling only the geometrical parameters of the scenarios (R_e, θ_c etc.).

The presented impulse responses of the rays have a very simple form, given by a sum of exponential functions. Therefore the obtained results are suitable for modeling of such UWB EM wave propagation in SPICE-like simulators. The great advantage of modeling in SPICE is a possibility of including detailed models of a transmitter and a receiver that consider their nonlinearities. Moreover in simulations of an EM wave propagation we can implement very fast and effective convolution algorithms with any input signal [9] or algorithms implementing only analytical calculations.

APPENDIX I – DEFINITIONS OF VARIABLES USED IN THE PAPER

The definitions of variables used in the paper are as follows:

$$T_c = \frac{1}{\sqrt{[a\cdot sin(\gamma')]^2 + [b\cdot cos(\gamma')]^2}} \times \frac{1}{\sqrt{[a\cdot sin(\gamma)]^2 + [b\cdot cos(\gamma)]^2}}, \tag{23}$$

$$F_c = \left| \int_{\gamma'}^{\gamma} \frac{1}{\sqrt{[a\cdot sin(\gamma)]^2 + [b\cdot cos(\gamma)]^2}} \right| d\gamma, \tag{24}$$

where:

$$\gamma' = arctan\left[\frac{b}{a} tan(\varphi')\right], \tag{25}$$

$$\gamma = arctan\left[\frac{b}{a} tan(\varphi)\right]. \tag{26}$$

where φ' and φ are the geometrical angle coordinates of the attachment (source point) Q' and the shedding point Q, respectively.

References

[1] M.Z. Win D. Porcino, W. Hirt , "Ultra-wideband radio technology: potential and challenges ahead", *IEEE Communications Magazine*, July 2003, pp. 2-11..

[2] Yan Zhao, Yang Hao, Member, Akram Alomainy, Clive Parini, "UWB On-Body Radio Channel Modelling Using Ray Theory and Sub-band FDTD Method", IEEE Transactions On Microwave Theory and Techniques, vol. 54, no. 4, June 2006, pp.1827 – 1835.

[3] M. Ghaddar, L. Talbi, T. A. Denidni, A. Sebak, "A Conducting Cylinder for Modeling Human Body Presence in Indoor Propagation channel", *IEEE Transactions on Antennas and Propagation*, vol. 55, no. 11, November 2007, pp. 3099-3103.

[4] Hsi-Tseng Chou, P. H. Pathak, P. R. Rousseau, "TD-UTD Solutions for the Transient Radiation of Pulsed Antennas Placed on PEC smooth Convex Surfaces", *IEEE Transactions on Antennas and Propagation*, vol. 59, no. 5, May 2011, pp. 1626-1637.

[5] P. H. Pathak, R. G. Kouyoumjian, "The radiation from Apertures in Curved Surfaces", N*ational Aeronautics and Space Administration*, Washington, D. D, July 1973,

[6] B. Gustavsen, A. Semlyen, "Rational approximation of frequency domain response by vector fitting", *IEEE Transactions on Power Delivery*, vol.14, no. 3, 1999, pp. 1052-1061.

[7] D. A. McNamara, *Introduction to the uniform geometrical theory of diffraction*, Artech House, Boston, London, 1990.

[8] P. Górniak, W. Bandurski, *A New Universal Approach to Time-Domain Modeling and Simulation of UWB Channel Containing Convex Obstacles Using Vector Fitting Algorithm*, IEEE Transactions on Antennas and Propagation, Vol. 62, No. 12, 2014, pp. 6394-6405.

[9] W. Janke, G. Blakiewicz, "Semi Analytical Recursive Algorithms for Convolution Calculations", in *Proc. IEE - Circuits, Devices and Systems*, vol. 142, no. 2, April 1995, pp. 125-130.